A new approach to enhance the reclaimed asphalt pavement features: role of maltene as a rejuvenator

Zaid Hazim Al-Saffar, Haryati Yaacob, Mhmood Khleel Saleem, Mohd Khairul Idham Mohd Satar, Ramadhansyah Putra Jaya, Munder Bilema, Choy Jau Lai & Mohd Zul Hanif Mahmud

Published online: 14 Oct 2021.

Submit your article to this journal

View related articles

View Crossmark data

Check for updates

A new approach to enhance the reclaimed asphalt pavement features: role of maltene as a rejuvenator

Zaid Hazim Al-Saffar[a,b], Haryati Yaacob[a], Mhmood Khleel Saleem[c], Mohd Khairul Idham Mohd Satar[a], Ramadhansyah Putra Jaya [d], Munder Bilema[e], Choy Jau Lai[f] and Mohd Zul Hanif Mahmud[a]

[a]Faculty of Engineering, School of Civil Engineering, Universiti Teknologi Malaysia, Skudai, Malaysia; [b]Building and Construction Engineering, Technical College of Mosul, Northern Technical University, Mosul, Iraq; [c]Department of Chemical industry, Mosul Technical institute, Northern Technical University, Mosul, Iraq; [d]College of engineering, Department of civil engineering, Universiti Malaysia Pahang, Gambang, Malaysia; [e]Department of Highway and Traffic Engineering, Faculty of Civil Engineering and Environmental, University Tun Hussein Onn Malaysia, Batu Pahat, Malaysia; [f]Department of Bioprocess and Polymer Engineering, School of Chemical and Energy Engineering, Universiti Teknologi Malaysia, Skudai, Malaysia

ABSTRACT

The properties of aged asphalt can be renewed using rejuvenating agents. Rejuvenators can improve the performance of reclaimed asphalt pavement (RAP) by reducing the asphaltene-to-maltene ratio back to their initial state. This study assessed the function of maltene as a rejuvenator to renew aged asphalt. Penetration, softening point, ductility and viscosity tests were performed to determine the ideal maltene content to be incorporated into RAP. The rejuvenated asphalt samples were evaluated using rolling thin film oven (RTFO), dynamic shear rheometer (DSR), bending beam rheometer (BBR), Fourier transform infrared (FTIR), thermogravimetric (TGA) and atomic force microscopy (AFM) measurements. The outcomes were compared with virgin and aged asphalts. Both oxygenated groups and asphaltene content decreased by adding 12% maltene. Essentially, DSR, BBR, TGA, and AFM analyses divulged the comparable performance of rejuvenated asphalt with virgin asphalt, signifying the potency of maltene for practical applications.

1. Introduction

Valuable and non-renewable natural resources, particularly asphalt binders and aggregates contained in asphalt mixtures, are extensively used in road pavements at annual basis (Celauro et al., 2010). The production of one tonne of hot-mix asphalt (HMA) was reported to consume 99 KWh (356 MJ) of energy, along with 23.8 kg of CO_2 emission (Hu et al., 2019). Road infrastructure maintenance, indisputably, exerts detrimental effects on the environment due to the massive amount of waste and debris generated from deteriorated pavements (Celauro et al., 2010). In order to surmount these emerging issues linked with extensive use of natural resources, as well as to improve the sustainability of pavement construction in terms of carbon footprint and energy use, it is pertinent for the asphalt industry to incorporate recyclable waste materials (Al-Bayati et al., 2018; Poulikakos et al., 2017).

Studies have reported that milling end-of-life pavements enables the re-use of aged and deteriorated pavement, such as the incorporation of reclaimed asphalt pavement (RAP) in producing asphalt

---

CONTACT Haryati Yaacob ✉ haryatiyaacob@utm.my

mixtures, wherein the role of rejuvenating agents becomes integral (Aurangzeb et al., 2014; Ingrassia et al., 2019; Noferini et al., 2017). The primary aim is to yield a rejuvenated asphalt mixture that resembles the virgin asphalt (VA) mixture. The use of RAP in HMA is highly cost-effective (Su et al., 2009; Yang et al., 2015) with less exploitation of the VA and aggregates (Blanc et al., 2019), thus implying vast environmental and economic benefits (Hussein et al., 2020a). Nonetheless, the chemical composition, as well as the physical and rheological properties of the RAP binder (aged asphalt), may change due to binder volatilisation and oxidation, which cause the binder to become stiff. This issue of stiffness is ascribed to the conversion of maltene fraction in asphalt into a more viscous asphaltene fraction (Firoozifar et al., 2011; Ma et al., 2015; Mansourkhaki et al., 2019; Rodríguez-Fernández et al., 2019).

Rejuvenating agents are incorporated not only to restore the properties of aged asphalt, but also to reverse the impact of ageing by increasing the contents of aromatic and resin in asphalt, thus decreasing the relative content of asphaltene (Elseifi et al., 2011; Hussein et al., 2020b). As a result, the viscosity and the stiffness decrease, while the penetration increases, rendering the asphalt to be more ductile that enables a performance as close to the original as possible (Al-Saffar et al., 2021; Ali et al., 2016; Zhang et al., 2019). Yu et al. (2014) reported that using high quantities of resin and aromatic fractions can enhance the rejuvenating effect. The literature depicts that numerous types of waste and by-product materials have been applied as rejuvenating agents, such as vegetable oil (VO), vegetable grease (VG), cooking oil (CO), organic oil, engine oil (EO), the EO bottom, distilled tall oil, naphthenic flux oil, aromatic extracts, and paraffinic base oil, and bio-oil (Cao et al., 2018; Zargar et al., 2012; Zaumanis et al., 2013, 2014a; Zhu et al., 2017).

It is noteworthy to highlight that several materials are unsuitable to function as rejuvenating agents due to their potential rutting damage when incorporated into the pavements (Zaumanis et al., 2014b). For instance, waste engine oil (WEO) and some petroleum-based products are beneficial only to boost asphalt performance at low temperatures, but unsuitable at high temperatures due to extreme softening of oil and ineffective aggregates-asphalt binding (Borhan et al., 2007; Jia et al., 2015; Wang et al., 2018). Some other factors that promote rutting damage are low stiffness of rejuvenated asphalt surface micro-layer, as well as incompatible and ineffective blending between rejuvenating agent and aged asphalt (Zaumanis & Mallick, 2015). Hence, the following should be considered when selecting a rejuvenating agent: (1) improvement in low-temperature properties of aged asphalt, and (2) does not adversely affect the performance at high temperature. Additionally, the rejuvenating agent must be able to mobilise and diffuse in aged asphalt so that a uniformly coated mixture is produced (Zaumanis et al., 2014b).

The durability of rejuvenating agent, nonetheless, presents another issue as the presence of volatile compounds in some softening agents could reduce asphalt stiffness to enable the eventual compaction and further improvement (Elkashef & Williams, 2017). Once the compounds are volatilised, the softening agents can no longer enhance the mixture. Therefore, it is integral to ensure that the rejuvenating agent has an enduring effect on the characteristics of asphalt mixtures. Apart from durability, the chemical interaction between a rejuvenating agent and asphalt is a vital factor as the former may accelerate ageing and make asphalt unusable (Elkashef & Williams, 2017). For instance, heavy fuel oils can volatilise at high recycling temperature and limit the RAP content in asphalt mixture to lower than 30% (Ji et al., 2017). Interestingly, the same rejuvenating agent can act differently in different asphalts. The aromatic extract, for example, can lead to higher efficiency when used with asphalt (PG58-10) as opposed to asphalt (PG58-28), where less efficiency was noted in the latter (Yu et al., 2014). Poor practicality or durability displayed by some rejuvenating agents for their medium – to long-term usage poses several shortcomings (Kaseer et al., 2019). Plant oils (triglycerides), for instance, can decompose into smaller compounds in the presence of water, moisture, oxygen, ultraviolet (UV) radiation, and bacteria (Bylikin et al., 2014; Fursule, 2008). Thus, extreme caution must be exercised when using plant oils as rejuvenators.

A previous study discussed the potential of maltene as a rejuvenating agent in aged asphalt, but the study only conducted basic tests rather than advanced tests to assess the rheological and chemical properties of the rejuvenated asphalt (Hussein et al., 2020b)

Given the above depiction, this present work investigated the potential of fresh asphalt-derived maltene to rejuvenate aged asphalt. Maltene (composed of high percentages of aromatic and resin, but a low percentage of saturates) was selected in this study due to its notable characteristics, in comparison to other rejuvenating agents. Aromatics in maltene increase the flexibility of asphalt, whereas resins promote anti-rutting ability. Other notable characteristics found in maltene are optimum viscosity, available in abundance, affordable, and applicable from laboratory to industrial setting. Maltene, being a key element in crude oil and asphalt materials, can easily derive from the asphaltene separation refinery units. The incorporation of maltene increases the percentage of RAP materials in mixtures and decreases the optimum amount of VA that should be included into the asphalt mixtures. Maltene has good blending and dissolution inside the asphalt structure that ascertains uniformity and compatibility, thus making it a practical rejuvenating candidate.

This present study is part of a wider research focus that had looked into the performance and durability of recycled asphalt mixtures. Penetration, softening point, ductility, viscosity, and flow activation energy were assessed to determine the optimal amount of maltene to be incorporated into asphalt. These tests were carried out on all types of samples that had a range of maltene percentages. Several tests, including maltene and asphaltene ratios, rolling thin film oven (RTFO), dynamic shear rheometer (DSR), bending beam rheometer (BBR) and Fourier transform infrared (FTIR) were performed on virgin, 100% aged, 40% aged, and rejuvenated asphalts. In order to determine the thermal stability of the selected asphalt samples, thermogravimetric analysis (TGA) was conducted, whereas the surface morphology and micromechanical characteristics of the asphalt samples were evaluated using atomic force microscopy (AFM).

2. Experimental

2.1. Raw materials for sample preparation

2.1.1. Virgin and aged asphalt

Penetration grade 60–70 asphalt was chosen as the VA in this study. This material was procured from a company that frequently supplies asphalt for roadwork in Malaysia, namely, Kemaman Bitumen Company (KBC) Malaysia Ltd. Table 1 lists the characteristics of VA used in this study.

The RAP was obtained from a surface layer in Yong Peng highway in the direction leading to Pagoh, Malaysia, through a milling process. The aged asphalt was extracted from the RAP using a two-step procedure. First, the recovered asphalt binder from the RAP was extracted using a methylene chloride solvent per ASTM D2172 (2017b). Then, the methylene chloride was separated using a rotary evaporator, and the aged asphalt was recovered per ASTM D5404 (2012b). The characteristics of the aged asphalt are listed in Table 1. To ensure consistency in terminology, 'aged asphalt' is the term used henceforth instead of 'recovered asphalt binder'.

2.1.2. Rejuvenator

Maltene was used as the rejuvenator in this study. The results of the elemental analysis of maltene, as well as its viscosity and specific gravity, are provided in Table 2. The extraction process of maltene was achieved via several stages, as shown in Figure 1. Petroleum ether (consists of light compounds

Table 1. The characteristics displayed by virgin and aged asphalts.

Properties	Virgin asphalt	Aged asphalt	Standard method
Density (gm/cm^3)	1.02	1.03	ASTM D70
Penetration (dmm.) at °C	64	18.5	ASTM D5
Softening Point (°C)	51.5	73	ASTM D36
Ductility (cm)	116	9	ASTM D113
Viscosity @ 135°C (mPa.s)	650	3500	ASTM D4402
Viscosity @ 165°C (mPa.s)	200	700	ASTM D4402

Table 2. Elemental composition and technical performance of maltene rejuvenator.

Item	C (%)	H (%)	N (%)	S (%)	O(%)	Density (gm/cm^3)	Viscosity (mPa.s)
Maltene	81.6	11.61	0.48	5.4	0.9	0.955	42.97@ 95°C
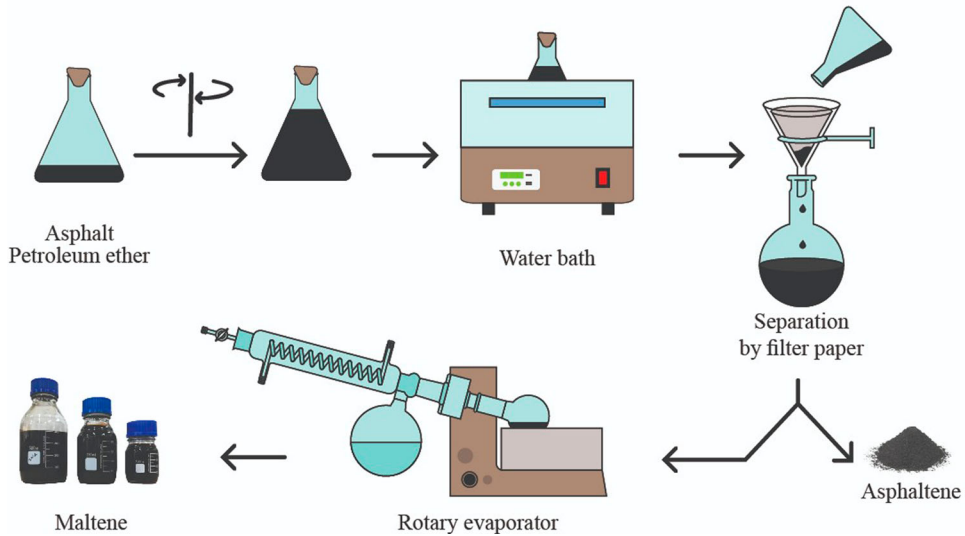
Figure 1. The procedure for extracting maltene.

Table 3. Comparison between the usage of petroleum ether and n-Heptane.

	100 mL n-Heptane (ASTM D4124)		5 mL Petroleum ether	
	Maltene (%)	Asphaltene (%)	Maltene (%)	Asphaltene (%)
1 g asphalt	80.97	19.03	80.83	19.17

with aliphatic hydrocarbons) was used to separate asphaltene from maltene. It has a low density and its boiling point ranging from 60 to 80°C. Thus, a small amount of petroleum ether can be used to separate asphaltene from maltene. In contrast, *n*-heptane (as an example) has a boiling point value that exceeds 98°C. Its density is higher than that of petroleum ether. Therefore, a higher amount of *n*-heptane is required to separate asphaltene from maltene, compared to petroleum ether. Hence, petroleum ether was selected as a solvent to separate asphaltene from maltene.

First, the VA was mixed with an optimum dose of petroleum ether (functioned as chemical solvent) in a container, and then placed in a water bath at 50°C with continuous stirring for 2 h until the soluble fraction was dissolved. Later, the mixture was kept in a water bath for approximately 60 min to let the asphaltene settle to the bottom from the dissolved virgin asphalt. After that, the asphaltene was filtered entirely out of the mixture. Next, the maltene was recovered at 50–70°C from petroleum ether using a rotary evaporator. Repeated recycling of the petroleum ether was possible depending on the extraction conditions, making the approach more economical. Finally, in order to eliminate the presence of chemical solvents completely, the maltene was heated in an oven at 80°C for 30 min. The results were compared with ASTM D4124 (2018), which assumed mixing 100 ml of *n*-heptane as solvent to 1 g of asphalt, to ensure that the process was successfully performed. Table 3 shows that asphaltene content obtained from asphalt binder using *n*-heptane was 19.03%, which is very close to that obtained via petroleum ether (19.17%).

Table 4. Types of asphalt used in this study.

Binder types	Asphalt binders
VA	Virgin asphalt binder, penetration grade (60-70)
100RA	100% RAP asphalt binder (aged asphalt)
40RA	40% RAP asphalt binder +60% virgin asphalt
40RA+4MLT	(40% RAP asphalt +60% virgin asphalt) + 4% maltene
40RA+8MLT	(40% RAP asphalt +60% virgin asphalt) + 8% maltene
40RA+12MLT	(40% RAP asphalt +60% virgin asphalt) + 12% maltene
40RA+16MLT	(40% RAP asphalt +60% virgin asphalt) + 16% maltene

2.2. Sample preparation protocol

In this step, the 40% aged asphalt was added to 60% of the VA and the sample was mixed with maltene at 135°C in a mixer with a rotation speed of 1000 rpm for 20 min to obtain a homogeneous blend. It was found that 40% of aged asphalt is the most common percentage used in recycled asphalt pavement (Ali et al., 2016). A trial-and-error approach was employed to choose the variables of time, temperature, and speed, which are the major determinants of how effectively VA, aged asphalt and maltene have blended. In the preliminary study, a maltene content of 4%, 8%, 12% and 16% of the overall weight of the asphalt was used for blending. Seven types of asphalt binders were used in this research, as shown in Table 4.

2.3. Sample characterisation

2.3.1. Penetration test
Penetration is the distance or depth (tenths of a millimetre) at which a standard needle weighing 100 g can vertically penetrate a sample at 25°C for 5 s. A penetration test was conducted to evaluate the hardness of the asphalt samples in accordance with ASTM D5/D5M (2013). Then, the average of three readings was recorded for each sample.

2.3.2. Softening point test
The softening point indicates the thermal sensitivity of asphalt. The test was carried out based on ASTM D36/D36M (2014). It indicates the behaviour of asphalt with temperature increases. The softening point was established at an average temperature at which the asphalt became sufficiently soft to enable 3.5 g of steel balls to fall from a specified height and touched the base plate. The thermal susceptibility of asphalt decreased with increment in softening point.

2.3.3. Ductility test
This test delineates the ductility of the asphalt material by measuring the degree of elongation of the asphalt material before breaking when the sample is dragged at a specified speed and temperature (5 cm/min at 25°C). The procedure was conducted according to ASTM D113 (2017a), where the length of the asphalt stretch prior to breaking was recorded.

2.3.4. Asphaltene and maltene ratios
Asphaltene and maltene ratios were measured to determine how the rejuvenator and various chemical fractions in the asphalt samples affect the rejuvenation mechanism. The test was done via a solvent extraction method using *n*-heptane per ASTM D4124 (2018). An *n*-heptane solvent was added to the samples at a 100:1 v/v ratio according to mass, after which the blend was heated and stirred with a magnetic stirrer and a hot plate for 45 min. Then, the scattered mixture was left for 60 min to reach ambient temperature. The next step was to filter the sample solution and wash the asphaltene remaining on the filter paper with extra solvent until the filtrate turned colourless. Then, the sample was dried in an oven at 107 °C until a constant weight is achieved. Equation (1) was used to determine the mass

percentage of normal-heptane insoluble (NHI) as the percentage by weight of the initial sample.

$$NHI, \% = A/B*100 \tag{1}$$

A and B: the overall mass of insoluble and the overall sample mass respectively

2.3.5. Viscosity test
Viscosity reflects the flow resistance and internal friction of asphalt; it was measured based on ASTM D4402/D4402M (2015). In this study, viscosity was determined at different temperatures, i.e. 135, 150, and 165°C with a Brookfield Thermosel viscometer. A cylindrical spindle was inserted into the asphalt sample at a constant temperature and rotational speed of 20 r/min. The torque measurements of the spindle were used to determine rotational viscosity. Low friction between spindle and asphalt sample indicated low viscosity and vice versa.

2.3.6. Flow activation energy
Recent studies have investigated the characteristics of asphalt binders and mixtures based on the notion of activation energy (Pellinen et al., 2004; Salomon & Zhai, 2002). The rotational viscosity of the different asphalt types in this study was assessed at 135, 150, and 165°C with a shear rate of 20 r/min to determine the workability of asphalt and its resistance to flow. The viscosity-temperature relationship was investigated based on the Arrhenius equation (Equation 2) (Salomon & Zhai, 2002).

$$\ln \eta = Ef/(RT) + \ln A \tag{2}$$

η: asphalt rotational viscosity (Pa. s); Ef: the viscous-flow activation energy (kJ. Mol^{-1}); R: the universal gas constant ($8.314 * 10^{-3}$ kJ.mol^{-1}. K^{-1}); T: the temperature (K); and A: empirical constant.

2.3.7. Rolling thin film oven (RTFO) test
A rolling thin film oven (RTFO) was used to conduct an experimental simulation of asphalt ageing within the short term, according to ASTM D2872 (2012a). A 35 g of asphalt was poured into each RTFO bottle. The bottles were then fixed in the rotating carriage of RTFO. The temperature was set to 163°C, and the experiment was run for 85 min with the airflow into each bottle at 4000 mL/min. The findings revealed that ageing occurred during the production and construction of HMA (Southern, 2015). The original mass and the final mass of the asphalt were weighed, and the loss of mass ought to be less than 1% following short term ageing (AASHTO T240, 2013).

2.3.8. Dynamic shear rheometer (DSR) test
The rheological and viscoelastic properties of the asphalt samples were evaluated using a DSR test at temperatures ranging from 46 to 76°C, with a step increase of 6 °C in accordance with ASTM D7175 (2015b). By measuring the complex shear modulus (G*) and phase angle (δ), the DSR test enabled the assessment of the rheological features of the asphalt binder, especially its ability to withstand rutting or irreversible deformation denoted as G*/sin δ (Zhang et al., 2019). Comprising an elastic (recoverable) element and a viscous (non-recoverable) element, G* denotes the resistance of a sample to deformation as the whole under recurring shear. Meanwhile, δ denotes the time discrepancy between the applied shear stress and the sequential shear strain, whereas increasing in δ indicates an increase in the viscous part of the viscoelastic behaviour. Therefore, rutting in hot mix asphalt can be anticipated based on these two parameters (G* and δ). The study used a loading frequency of 1.59 Hz to simulate a traffic speed of around 90 km/h (Lillian Gungat et al., 2018).

A single spindle was included in the DSR device with a 25-mm plate-plate geometry, which was considered appropriate for assessing resistance to rutting at high temperatures ($\geq$ 46°C). The test required the insertion of 1-mm thick asphalt samples between the two plates. The particular failure conditions of $\geq$ 1.0 kPa were applied during testing.

2.3.9. Bending beam rheometer (BBR) test

The potential of the asphalt binder to crack at low temperatures was assessed via the Bending Beam Rheometer (BBR) test, which quantifies the m-value and creep stiffness S(t) of the asphalt sample at reduced temperature. In this study, the cracking performance of the asphalt samples was evaluated based on ASTM D6648 (2016). The procedure involved employing a 12.5 mm × 6.25 mm × 127 mm asphalt beam at temperatures of $(-6, -12, -18, -24)°C$ with a load weighing 0.98 N under normal gravity and under a 60-sec loading time. To guarantee resistance to cracks at low temperatures, the Superpave specification included a 300-MPa maximum value for S(t) and a minimum m-value of 0.30.

2.3.10. Fourier transform infrared (FTIR)

Chemical functional groups are distinguished by a singular infrared absorption characteristic, which is why functional groups in asphalt can be efficiently identified via FTIR analysis (Feng et al., 2016). The chemical changes as well as the FTIR outcomes of the asphalt samples were analyzed with an IRTracer-100 device displaying a 0.25 cm^{-1} resolution and fast 20 spectra/second scanning. Based on the literature (Hofko et al., 2017), all samples were preheated for a few minutes to be sufficiently workable for sample preparation. Then, the optics were cleaned with an organic solvent to remove any remaining binder and the acetone was added to remove any remaining solvent. A small mass of preheated asphalt sample was taken by a spatula and then applied directly onto the FTIR optics. The procedure involved an infrared beam penetrating the IR-transparent, high-refractive index, ATR crystal prism, to achieve complete reflection at the crystal-sample interface at a 600–3000 cm^{-1} wavenumber. Chemical functions can be distinguished based on the intensity and frequency of light absorbed, which dictates the absorption of various bonds. Peak height is produced from the captured chemical functional group in the absorbance or transmittance forms and the band area within an FTIR spectrum. In this way, the concentration of a particular bond in the sample can be determined. The TQ analyst EZ Edition software was used to facilitate data collection and measurement of functional group band areas. An accurate integral value for every area was attained as shown in Figure 2.

According to the literature (Ghavibazoo et al., 2013; Hofko et al., 2018; Mirwald et al., 2020a; Yan et al., 2016), susceptibility to oxidation is exhibited especially by oxygenating functional groups (e.g. carbonyl, sulfoxide). Spectral bands at about 1700cm^{-1} and 1030 cm^{-1} illustrate carbonyl and sulfoxide absorbance, respectively (Huang & Turner, 2013), so they are often used to analyze binder ageing.
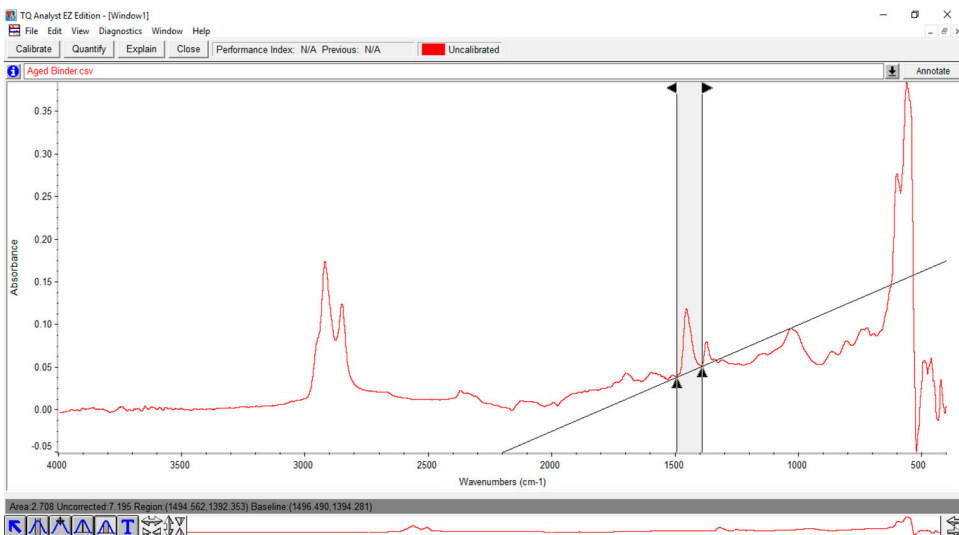

Figure 2. TQ analyst EZ Edition software used to determine IR spectra absorbance band area.

The approach proposed by Lamontagne et al. (2001) was employed to determine the functional and structural indices of the samples based on the calculated valley-to-valley band areas. Equations (3–6) were used to determine several particular band area-based indices obtained from the infrared spectra (Mouazen et al., 2011; Mouillet et al., 2008; Yan et al., 2016).

$$\text{Carbonyl index} = A1700/\left(\sum A\right) \tag{3}$$

$$\text{Sulphoxide index} = A1030/\left(\sum A\right) \tag{4}$$

$$\text{Aromaticity index} = A1600/\left(\sum A\right) \tag{5}$$

$$\text{Aliphatic index} = (A1376 + A1460)/\left(\sum A\right) \tag{6}$$

where the area equivalent to 700-3000 cm^{-1} spectral band is denoted by $\sum A$.

2.3.11. Thermogravimetric analysis (TAG)

TGA was conducted with a TGA Q500 device in line with ASTM E1131(2014). The process involved exposing every sample (1 mg) to nitrogen flow at a 10°C/min heating rate and a (30–900)°C temperature spectrum (Ciryle et al., 2016). The experimental output comprised sample TG and derivative curves (DTG) curves.

2.3.12. Atomic force microscopy (AFM)

The AFM imaging technique allows for high-resolution insight into the surface morphology and micromechanical qualities of materials. This method enables a micro-level observation of the interaction between the rejuvenating agent and the aged asphalt and how the former alters the latter. Therefore, AFM can further inform the researcher about the mechanism of rejuvenation of the aged asphalt (Yu et al., 2014). Contact, intermittent contact, and non-contact are the scanning modes employed in the AFM experiments. These modes are based on the size gap of the sample surface and the probe tip. The sample surface characteristics determine the most suitable mode. In this study, since the sample surface did not come into contact with the probe tip, and the gap between them was (0.1–10) nm, the non-contact mode was employed. A Smart SPM 1000 scanning probe microscope AIST-NT was used to assess the morphology of the asphalt samples with a 300-kHz drive frequency and a 0.5-Hz scan rate at room temperature and atmospheric pressure. Moreover, $50 \times 50\ \mu m$ images were obtained to observe the microstructure of the asphalt matrix.

3. Results and discussion

3.1. Penetration and softening point

Figures 3 and 4 show the impact of maltene as rejuvenator on the penetration and the softening point of aged asphalt, respectively. It can be clearly seen that the addition of aged asphalt can reduce the penetration and increase the softening point of asphalt. When asphalt ages, the light chemical components inside the asphalt transforms into heavy chemicals, thus leading to the increased ring-like structures that are packed and condensed, such as asphaltene (Wang & Ye, 2020). Consequently, penetration decreases and softening point increases as a result of a higher content of heavy components such as asphaltene. However, adding maltene to the blend resulted in a linear increase in penetration, reaching close to the desired 60/70 penetration grade. Meanwhile, when the maltene was added, the softening point decreased. These two observations could be attributed to the reduction in the asphaltene ratio caused by the maltene addition shown in Table 5. The asphaltene and maltene ratios were defined in line with ASTM D4124 (2018). It can be seen that the ratio of asphaltene in 40RA decreased with the addition of maltene. It must be noted, however, that it is impossible to completely restore
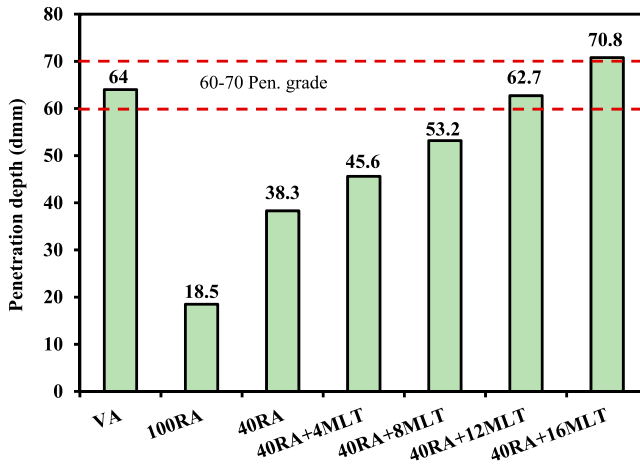
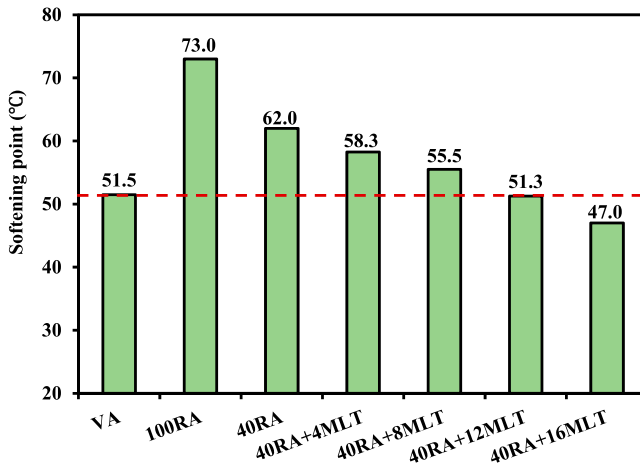**Figure 3.** Maltene contents dependent penetration variation of the obtained samples.

Figure 4. Maltene contents dependent softening point variation of the obtained samples.

Table 5. The asphaltene and maltene ratios of different asphalt types.

Type of asphalt	Maltene (%)	Asphaltene (%)
VA	80.97	19.03
100RA	67.90	32.1
40RA	75.54	24.46
40RA+12MLT	80.69	19.31

the initial qualities of the aged asphalt because the ageing it had undergone during service life has impacted its structure.

More specifically, at 25°C, 100RA had a penetration value of 18.5 dmm, while 40RA had a penetration value of 38.5 dmm. Meanwhile, 40RA+12MLT displayed a penetration value of 62.7 dmm, which was close to that of VA (64 dmm). Figure 4 portrays that 100RA and 40RA exhibiting softening point at 73°C and 62°C, respectively. However, the softening point of 40RA declined to 51.25°C when 12% maltene was added, which was very similar to that of VA.
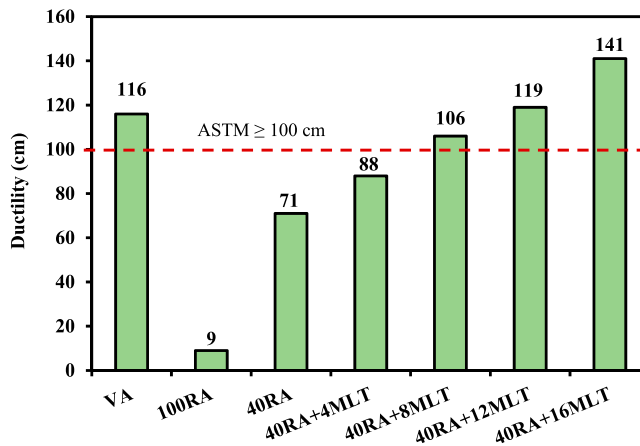
Figure 5. Maltene contents dependent ductility variation of the obtained samples.

3.2. Ductility

Figure 5 shows the effect of adding maltene on the ductility of the aged asphalt. The ductility of 100RA and 40RA appeared to be very low. The reason could be because the asphalt has been subjected to various circumstances during its service life, such as heat, pressure, air, humidity, rain, and ultraviolet (UV) rays. These factors lead to dehydrogenation, oxidation, and subsequently, the deterioration properties of asphalt. As a result, asphaltene content increased, while the oil and resin contents decreased, leading to an increasing in the brittleness that negatively affected the behaviour of the asphalt.

Incorporation maltene increased ductility, as the percentage of asphaltene diminished. The reason is that the addition of maltene compensated for the percentages of the components that had been lost due to the conditions mentioned above, hence rejuvenating the blend containing 40RA. More specifically, with the addition of 8% maltene, the ductility became higher than the ASTM specification ($\geq$ 100 cm) (ASTM D113, 2017a), whereas with the addition of 12% maltene, the ductility of 40RA+12MLT became marginally higher than that of VA. Thus, it can be concluded that maltene could enhance the ductility of aged asphalt while alleviating its stiffness.

3.3. Viscosity

The rotational viscosity of all asphalt samples is indicated in Figure 6. Compared to the 60/70 VA, the aged asphalt was significantly more viscous, so the blend hardened more easily, leading to a more viscous mixture. It has been realised that the presence of 10% or less of aged asphalt in the mixture has little influence on the viscosity and rheology of the mixture (Zaumanis et al., 2014a), but the asphalt blend viscosity can increase when the aged asphalt content exceeds 20% (Roberts et al., 1991). In this study, the addition of 40% aged asphalt had significantly increased the viscosity. Nonetheless, the addition of maltene caused a decrease in the rotational viscosity, as per Figure 6. At 135, 150, and 165°C, 100RA exhibited viscosities of 3500, 1400, and 700 mPa.s, respectively. At the same three temperatures, 40RA had a viscosity of 1550, 750, and 350 mPa.s, respectively. The asphaltene-maltene ratio during short – and long-term ageing-induced internal structural changes in the asphalt binder, and subsequently increased the viscosity of the aged asphalt. This caused the asphalt to harden with increased viscosity. Usually, asphalt ages during short-term ageing due to the construction process, which involves mixing, transport, and laying of asphaltic materials. Ageing is further facilitated at high temperatures (Moghaddam & Baaj, 2016). The oxidation and volatilisation of the asphalt and the reduction in oil constituents are the main factors that affect short-term ageing. Meanwhile, surface
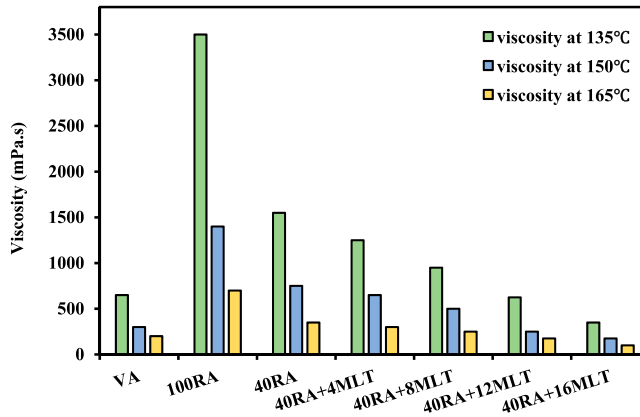
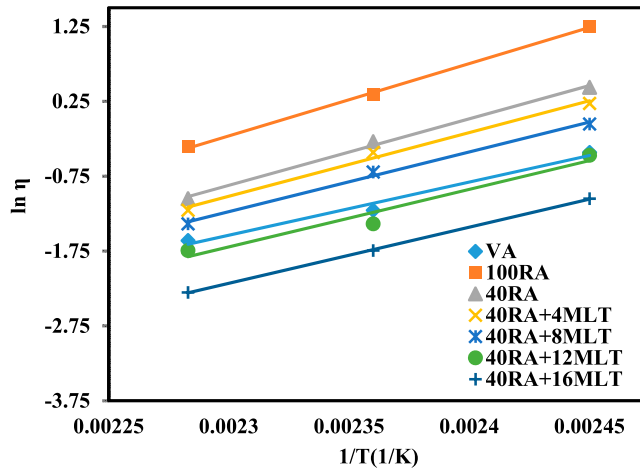**Figure 6.** Maltene contents dependent viscosity variation of the obtained samples.

Figure 7. Arrhenius plot for each type of asphalt binder.

layer polymerisation, oxidation, and photo-oxidation are the key factors affecting long-term ageing (Alvarez, 1994; Roberts et al., 1991; Zaumanis & Mallick, 2015).

Owing to the significant amount of aged asphalt content, 40RA had a different viscosity than VA. Furthermore, within the temperature spectrum of (135, 150 and 165)°C, 40RA+12MLT had a notably lower viscosity compared to the aged asphalts, similar to the VA viscosity. More specifically, 40RA+12MLT had a viscosity of 625 mPa.s at 135°C, 267 mPa.s at 150°C, and 175 mPa.s at 165°C. These observations suggest that the viscosity of a blend containing 40% of aged asphalt can be restored as it was initially via the addition of 12% maltene. Hence, it can be concluded that the addition of 12% maltene is ideal for achieving the desired 60/70 grade, based on the physical properties tests.

3.4. Flow activation energy

Pavement construction requires the asphalt to be workable, which can be ensured by increasing the fluidity of the asphalt binder, leading to a lesser energy requirement (Zhang et al., 2019). The binder's fluid temperature is reflected by its flow activation energy (Tan & Guo, 2013). Figure 7 provides the Arrhenius plot of all the asphalt samples within the temperature spectrum of (135–165)°C. The Ln η and l/T parameters were plotted to obtain the Arrhenius equation, where Ef/R and ln A respectively denote the intercept and slope of the equation. To determine the flow activation energy, Ef, ln A was multiplied by the universal gas constant, R. Lower activation energy indicates that the asphalt
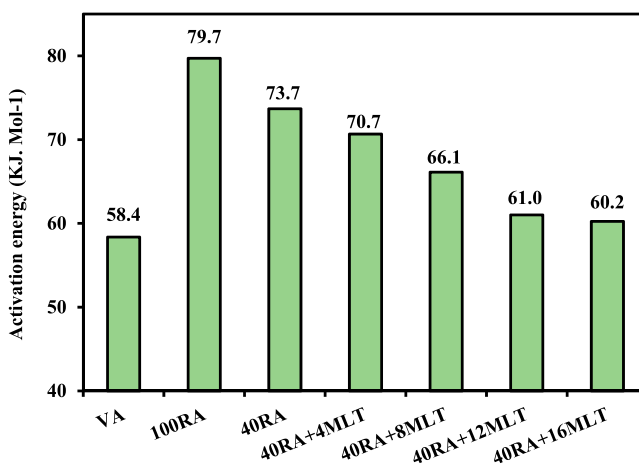
Figure 8. The activation energy for different asphalt samples.

binder is less sensitive to temperature changes, while higher activation energy shows a higher sensitivity to temperature changes. The activation energy of every asphalt sample in the temperature spectrum of (135–165)°C is listed in Figure 8. Ageing can increase the polar fractions, thus increasing the energy needed for the binder to flow, which is why the activation energy of 100RA exceeded that of VA (79.71 kJ.mol^{-1} vs. 58.37 kJ.mol^{-1}). Meanwhile, the activation energy of 40RA was 73.69 kJ.mol^{-1}. Ageing-induced stiffness was attenuated by the addition of maltene, which also decreased activation energy to be 61.02 kJ.mol^{-1} at 12% of maltene.

3.5. Mass loss after RTFO

This test simulates the effect of mixing, transporting, and compacting processes on asphalt hardening (Southern, 2015). Figure 9 indicates the volatilisation effect of asphalt ageing on RTFO, where a key concern when using the RTFO is the loss of volatiles. It is important to note that the lighter components in the asphalt sample may evaporate during the test, so that the asphalt sample may lose some material. 100RA and the 40RA demonstrated a mass loss of 0.19% and 0.56%, respectively. However, 40RA+12MLT and VA exhibited 0.95% and 0.76% mass loss, respectively. It is, therefore, obvious that more significant ageing occurred in VA and 40RA+12MLT because ageing had already occurred in the aged asphalt (Cavalli et al., 2018). Compared to the VA, the aged samples lost fewer volatiles and was less oxidised. Nevertheless, the mass loss of 40RA+12MLT was still less than 1%, thus complying with Superpave specifications. Moreover, as suggested by Zaumanis et al. (2014b), the partial distillation of a solvent from the maltene-rejuvenator during extraction could be the cause for the greater mass loss in the rejuvenated asphalt.

3.6. Dynamic shear rheometer (DSR)

3.6.1. Complex shear modulus (G∗)

The complex shear modulus, G∗, is the resistance to deformation during shear loading (Zhang et al., 2019), where resistance increases with an increase in the G∗ value (Zhu et al., 2017). Figure 10 shows that the 100RA and the 40RA had higher G∗ values compared to the VA and 40RA+12MLT because of the higher asphaltene content in the former resulting from oxidation during service life. A high G∗ value indicates a stiffer asphalt binder. Nevertheless, aged asphalt was softened via the addition of maltene; it was found that the addition of 12% maltene made the rejuvenated asphalt (40RA+12MLT)
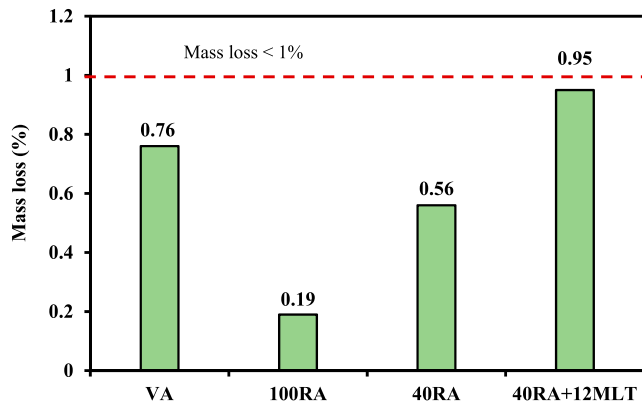
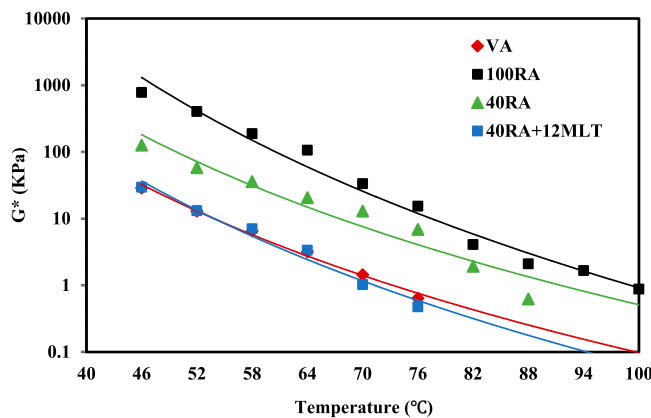**Figure 9.** Post-RTFO mass loss for the different binder types.

Figure 10. G∗ associated with the different binder types.

similar to VA in terms of shear deformation resistance. In summary, the complex modulus of the asphalt increased with increasing softening point, similar to the findings of previous works in this field.

3.6.2. Phase angle (δ)

The viscoelastic qualities of the asphalt can be assessed based on the phase angle (Zhang et al., 2018a). A full elastic material has no phase angle, that is, $\delta = 0$. Meanwhile, a fully viscous material has a $\delta = 90$, which denotes the phase angle of the stress and strain response (Wang & Ye, 2020). This means that a low δ value indicates a more elastic asphalt that more effectively recovers from shear deformation (Zhu et al., 2017). As per Figure 11, 100RA and 40RA had a lower phase angle than VA and 40RA+12MLT. When the phase angles at different temperatures (46°C to 76°C) were compared, the results showed that all the samples experienced an increase in phase angle with increasing temperature. Therefore, with increased temperature, the elasticity of the asphalt reduces. Thus, the viscosity property of the asphalt is more obvious at high-temperatures. Both 100RA and 40RA experienced less obvious reduction in phase angle at higher temperature, signifying that at high temperature, ageing did not exert a strong effect on the viscoelasticity ratio of the asphalt, per the results of many studies in the past (Wang & Ye, 2020). Meanwhile, the rejuvenated asphalt exhibited a marked increase in phase angle, even slightly exceeding the phase angle of VA. As a result, the addition of maltene rejuvenated the viscous components and restored the high-temperature resistance of aged asphalt close to the initial level. This finding supports the results of rotational viscosity.
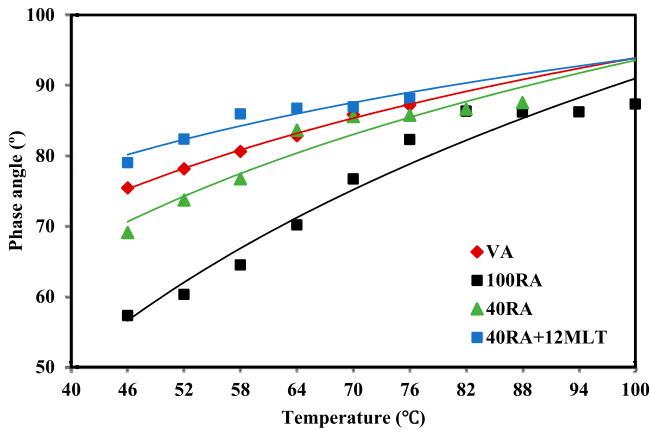
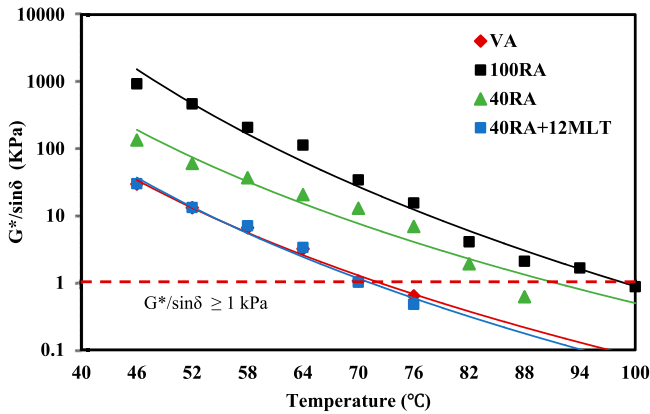**Figure 11.** δ of the different asphalt binder types.

Figure 12. The rutting index associated with the different binder types.

3.6.3. Rutting index

Figure 12 illustrates the rutting index of the different asphalt types. Good asphalt resistance to permanent deformation at high pavement temperature is indicated by a large rutting index. An increase in temperature leads to a reduced rutting index, thus increasing the softness of the asphalt and reducing its viscosity (Zhang et al., 2018a). Compared to the VA, the aged asphalts were significantly more resistant to rutting due to the stiffness inherent in ageing during service life. The failure temperature was 100°C and 88°C for 100RA and 40RA, respectively where the value of $G*/\sin\delta$ was less than 1.0 kPa. However, the asphalt rejuvenated with maltene was considerably less resistant to rutting compared to the aged asphalts, reflecting the ability of the maltene to improve the softness of aged asphalt. On the other hand, the rutting resistance of VA did not diminish as much as that of 40RA+12MLT. This result has two implications, namely, that maltene can restore aged asphalt and that the sensitivity of 40RA+12MLT to rutting at elevated temperatures is marginally higher compared to that of VA. However, studies have claimed that increased rutting sensitivity due to rejuvenator usage is still acceptable if the rejuvenator were employed in a suitable concentration and were spread and mixed thoroughly in the asphalt film (Zaumanis et al., 2014b). This case explains the failure of both 40RA+12MLT and VA at the same temperature (76°C).
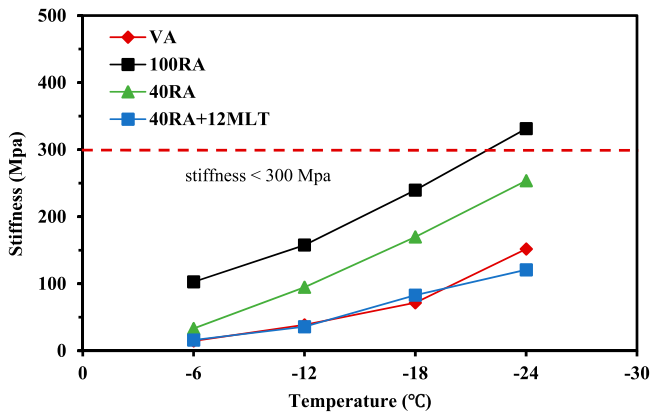
Figure 13. The relation between stiffness and temperatures for the asphalt binders.
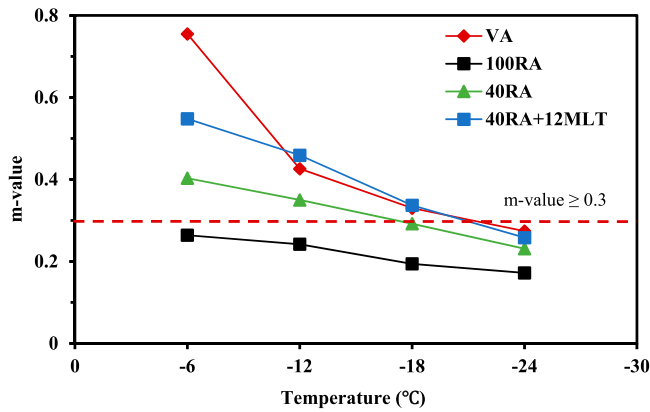

Figure 14. m-value results of the asphalt binders.

3.7. Low temperature cracking resistance

Resistance to cracking at low temperatures was assessed via the BBR test. The risk of such cracking is expected to diminish with a lower creep stiffness and a higher m-value (Wang et al., 2017). These two parameters are shown in Figures 13 and 14 with respect to the VA, the 100RA, the 40RA, and the 40RA+12MLT samples. The stiffness increased and the m-value decreased at a lower temperature, as anticipated. 100RA failed at −6°C and 40RA failed at −18°C, with an m-value < 0.3. The addition of maltene improved the resistance to cracking at low temperatures, as well as reduced the stiffness and increased the m-value. Aromatic content in maltene has the ability to decrease cracking in asphalt at low temperature. The Superpave binder must have a stiffness of less than 300 MPa and an m-value higher than 0.3. These requirements were fulfilled by both 40RA+12MLT and VA at (−6, −12, and −18)°C. On the other hand, neither of the asphalts met the requirements at −24°C because both their m-values were less than 0.3. Based on these comparable results, it can be deduced that 40RA+12MLT and VA exhibited near similar outcomes. Nonetheless, the VA sample recorded a slightly higher relaxation rate (m-value) than 40RA+12MLT.

3.8. Functional groups analysis

Figure 15 illustrates the FTIR spectra of maltene and different asphalt samples that ranged at 600–3000 cm^{-1}. The peaks exhibited notable changes in position and intensity, with every asphalt
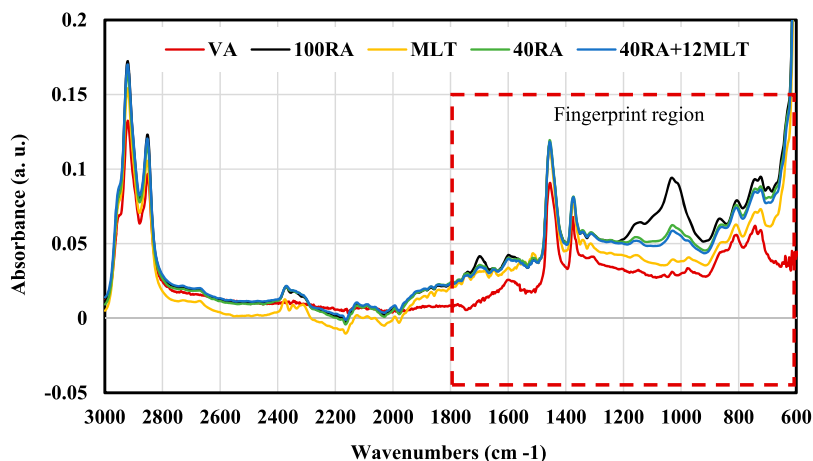
Figure 15. FTIR spectra of the selected samples.

sample displaying changes in the intensity of functional groups. In general, a wavenumber of around 722 cm^{-1} was associated with the bending vibration of long-chain methylene $-(CH_2)_n-$. Meanwhile, the C–C group was identified based on the fact that every binder exhibited a bending frequency at about 740 cm^{-1}. A bending frequency at approximately 812 cm^{-1} was also displayed. An asymmetric vibration of CH_2 and CH_3 were indicated by peaks at approximately 1460 and 1376 cm^{-1} in every asphalt sample. Moreover, the $S = O$ (sulfoxide) group was indicated by the absorption peak at approximately 1030 cm^{-1}. Additionally, the C–C (aromatics) band was signalled by a peak at approximately 1600 cm^{-1}, while $C = O$ (ketones or carboxylic acid) was signalled by a peak at around 1700 cm^{-1}. Asphalt samples displayed the C–H stretching vibration indicated by absorption bands at 2852 and 2920 cm^{-1} (Figure 15).

A comparison between the FTIR spectra of the different asphalt samples exemplified that the rheology of aged asphalt was affected by increased polarity induced by the functional groups which in turn, increased the stiffness (Mousavi et al., 2016). As a result, an elevated shift was noted in the spectra located at the fingerprint region (infrared spectrum at 650–1800 cm^{-1}). These findings are in agreement with Mirwald et al. (2020a, 2020b), who ascribed the increment in intensity to the increased asphaltene. Nonetheless, the addition of maltene led to a decreasing in the polarity and thus decreasing the stiffness of the aged sample. However, the peaks associated with oxidation-induced asphalt ageing did not disappear, although maltene was added to the aged asphalt. This is a non-reversible form of ageing, as recognised by Xiaohu and Isacsson (2002).

From the discussion, the alterations noted in the functional groups due to ageing were assessed based on the chemical ageing index (CAI) as shown in Table 6. The CAI was calculated by adding the indices of carbonyl and sulfoxide ($I_{C=O} + I_{S=O}$) (Al-Saffar et al., 2020). It can be seen that the CAI for VA was lower than those of other asphalt samples, as the CAI increased with the addition of aged asphalt. The reason is associated with increasing the carbonyl and sulfoxide groups due to the oxidation of aged asphalt during the service life. Nevertheless, incorporation of maltene into the matrix had decreased CAI due to the reduction in both $I_{C=O}$ and $I_{S=O}$, thus resulting in decreased ageing. The reduced asphaltene content in the 40RA+12MLT was also confirmed when compared the asphaltene and maltene ratios in 40RA+12MLT with 40RA and 100RA samples, as shown in Table 5.

On the other hand, in comparison to VA, the aged samples had a higher aromaticity index and a lower aliphatic index, as displayed in Table 7. The main reasons for these results are related to the dehydrogenation, condensation, and oxidation of aged asphalt. Thus, these findings explain why the aged asphalt is stiff. Furthermore, when maltene was added, the aromaticity index decreased and the aliphatic index increased as a result of reducing in the asphaltene content. The outcomes discussed

Table 6. The asphalt samples and their associated carbonyl, sulfoxide and CAI indices.

Type of asphalt	Carbonyl index ($I_{C=O}$)	Sulphoxide index ($I_{S=O}$)	Chemical ageing index (CAI)
VA	0.015	0.005	0.02
100RA	0.027	0.250	0.277
40RA	0.023	0.098	0.121
40RA+12MLT	0.016	0.080	0.096

Table 7. Aromaticity and aliphatic indexes of asphalt samples.

Type of asphalt	Aromaticity index	Aliphatic index
VA	0.0306	0.409
100RA	0.0432	0.252
40RA	0.0379	0.285
40RA+12MLT	0.0370	0.296
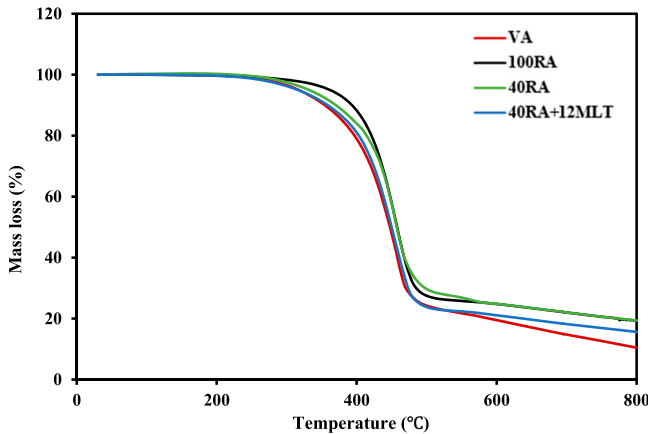
Figure 16. TG curves for asphalt binders.

above signify that adding maltene has softened the aged asphalt and increased the ageing resistance of the rejuvenated asphalt to some extent.

3.9. Thermogravimetric analysis (TGA)

The thermal stability of the different asphalt samples was examined using thermogravimetric analysis (TG) and the results shown in Figure 16. Three zones of weight loss can be clearly identified. The loss of mass was low in the first zone, terminating in an initial decomposition temperature (IDT) (Elkashef et al., 2018). The second zone showed a rise in thermal decomposition up to the highest mass loss for every type of asphalt at approximately 455°C, and followed by a steady decrease of the rate of breakdown until it was close to zero beyond 530°C. The third zone began by the almost horizontal plateau illustrated in Figure 16. The breakdown of carbonaceous materials in the solid residues was the cause of the degradation in the last zone at a temperature higher than 500°C (Bach & Chen, 2017). Figure 16 also proves that none of the components of asphalt samples would suffer notable decomposition during the process of production and mixing of the asphalt mixture. The reason is that the initial decomposition temperature (IDT) for all asphalt samples began at approximately 240°C, which is higher than the production temperature of HMA.
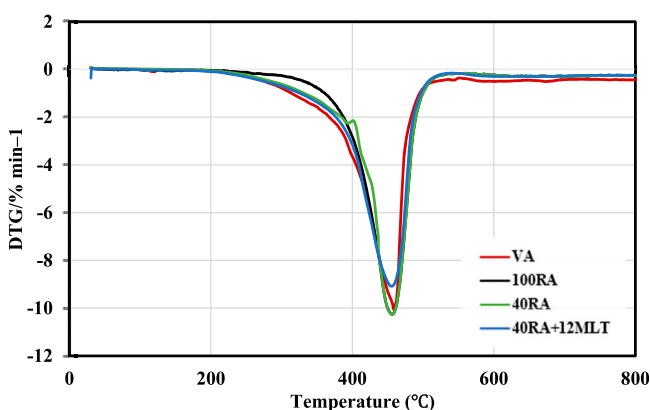
Figure 17. DTG curves for asphalt binders.

Table 8. IDT and char yield of asphalt samples.

	IDT/°C	Char yield %
100RA	270	27
40RA	265	25.75
VA	237	21.75
40RA+12MLT	235	22.5

Regarding the derivative thermogravimetric (DTG) curve, Figure 17 shows the rate at which mass loss changed as a function of temperature per the (DTG) curve. It can be seen that the greatest mass loss occurred at a temperature of approximately 455°C. After this temperature, the decomposition rate gradually declined until it reached almost zero at around 530°C. At this temperature, the loss of mass was negligible.

Changes in asphalt weight loss and breakdown correlated with the fractions of asphalt, in which the asphalt was composed of maltene (saturates, aromatic, and resin) and asphaltene. The lower amount of weight loss was observed in 100RA and 40RA, which contained the highest percentage of asphaltene. This result is attributed to the highest proportion of mass loss that occurred in both saturates and aromatics, and later followed by resins and asphaltene. This outcome is in line with that reported in prior studies (see Jiménez-Mateos et al., 1996; Tahmoorian et al., 2018), whereby the mass loss of asphalt could happen due to decomposition in saturates and aromatics at $T < 350$°C. Thereafter, the mass loss increased due to decomposition of resins and aromatics, as well as some percentages of asphaltene at $350 < T < 500$°C. Nevertheless, upon exceeding 500°C, substantial mass change in asphalt occurred due to decomposition of asphaltene. It is noteworthy to emphasise that both aromatics and resin decomposed within the same temperature range.

Table 8 shows that the aged asphalts recorded higher char yield percentage (the remaining mass after complete sample degradation) and IDT, in comparison to virgin and rejuvenated asphalts. The percentage of char yield and IDT, nonetheless, decreased due to the addition of maltene. This clearly implies that aged asphalts (100RA and 40RA) recorded higher thermal stability than virgin and rejuvenated asphalts (VA and 40RA+12MLT). The reason is that the former contained a higher level of asphaltene than the latter. No significant deviation in the 40RA+12MLT versus the VA was noted, as per the TG and DTG curves. It could thus be deduced that the blending of the rejuvenator (maltene) and the asphalt is successful; thus enabling the asphaltene to scatter better and the four asphalt fractions to regain their equilibrium (Elkashef et al., 2018)
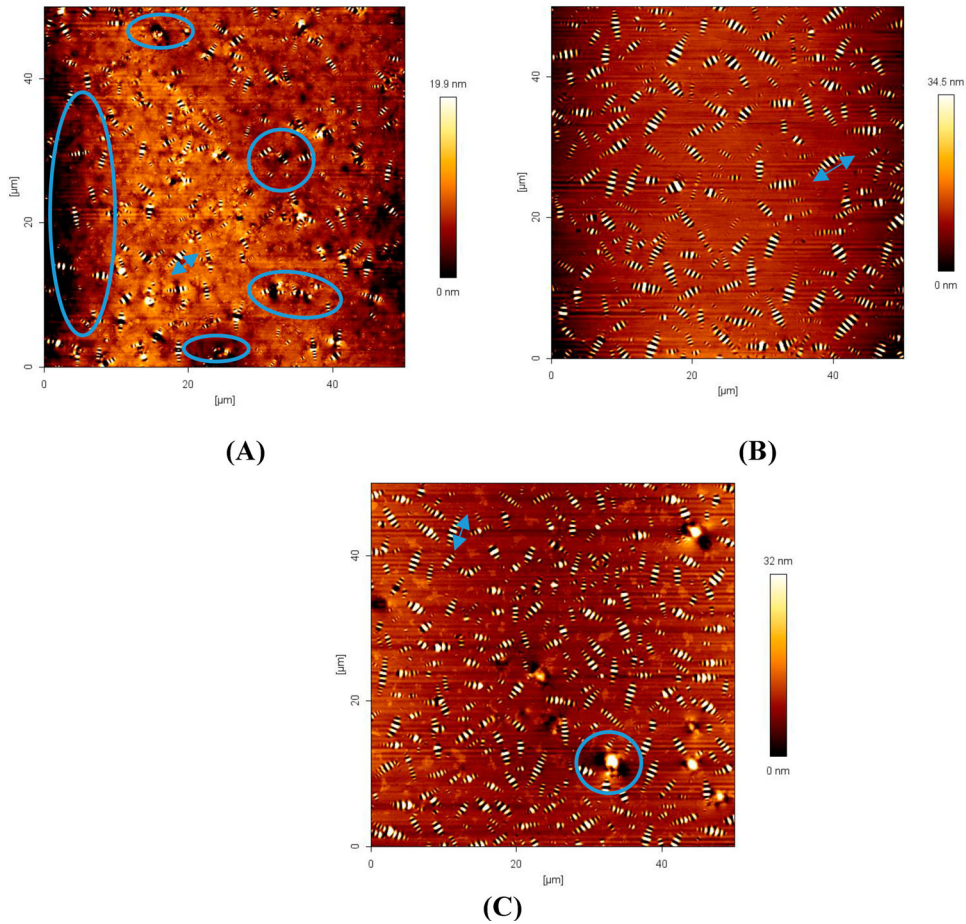
Figure 18. AFM images of (A) RA, (B) VA, and (C) 40RA+12MLT samples (Scanned area: $50 \times 50 \, \mu m^2$).

3.10. Atomic force microscopy (AFM) images

Figure 18 shows the microstructure of the asphalt samples investigated in this study. The samples exhibited different scan sizes because they had different microstructural characteristics. Two main phases were observed: a soft phase (light components in a continuous phase) and a rigid phase (dispersed phase randomly distributed in a 'bee-like' matrix).

The VA exhibited fewer, albeit longer, bigger, and more distinct 'bee-like' structures than aged asphalt. It was observed that 'bee-like' structures are formed due to the microcrystalline asphaltene and wax in asphalt (Pizzorno et al., 2014), whereas varied components in asphalt contribute to structural shapes, sizes, and topographies (Aguiar-Moya et al., 2017). The formation of these 'bee-like' structures could be due to other factors as well (Allen et al., 2014; Pauli et al., 2011), but the overriding factors refer to the content of wax and microcrystalline asphaltene in asphalt (Cuadri et al., 2014; Hofko et al., 2016).

On the other hand, the microstructure of aged asphalt revealed multiple black dots and dark areas as shown in Figure 18(b), attributable to the aggregation of polar components (Gong et al., 2016), which referred to the stiffness of asphalt. This phenomenon signified that the ageing process during the service life had a significant influence on the microstructure phases (Wang & Liu, 2017). The breakage of aged asphalt produced carbon or coal components, which could show up as black dots. This not only increased the softening point but also weakened the properties of asphalt as per the

physical properties tests. Based on the phase images, the dark area had more stiffness than the bright area. This result is in agreement with that reported by Zhang et al. (2018b), who noted that asphalt pavement could undergo uncontrolled thermal degradation and oxidation that could lead to undesirable results. For instance, the presence of C = C may induce oxidation. This bond is weaker and easier to break than the C–C bond. Asphaltic materials are characterised by double bonds, in which these bonds could also affect the characteristics of asphalt. Oxidation either causes an increase in oxygen or a decrease in hydrogen, or both concurrently. Stiffness and brittleness are bound to increase with increased oxygen content. Increment in hydrogen seemed to increase both carbon content and stiffness. Overall, this process influenced the rheological properties of the asphalt.

Figure 18(c) illustrates that the addition of maltene to aged asphalt had reversed the effect of ageing while simultaneously restoring the properties of asphalt to some extent. The images of 40RA-12M closely resembled those of VA, which signified the effect of maltene on the rheological and morphological properties of aged asphalt. Nevertheless, it seemed impossible to completely return the rejuvenated asphalt to the microstructures of VA. The black dots were observed to greatly reduce, possibly because it prevented the highly-oxidized components in the aged asphalt from aggregating thus rejuvenating asphalt. The rejuvenated asphalts displayed a larger 'bee-like' structure than that in aged asphalt. This implies that changes in the molecular composition of asphalt did alter the size and shape of the 'bee-like' structure.

These findings are in agreement with those reported by Magonov et al. (2017) and Backx et al. (2014). The differences in the dispersed phase (bee-like structure) and the continuous phase are attributed to the different contents of asphaltene, resin, saturates, and aromatics in asphalt samples. The characteristics of the maltene (rejuvenator) appeared to have a crucial role as well.

4. Conclusion

Based on the detailed experimental results, analyses, comparison and discussion, the following conclusions are drawn:

(1) The addition of maltene to the blend containing 40% aged asphalt caused a reduction in the viscosity and softening point as well as an enhancement in the penetration and ductility. Consequently, the mixing temperature of asphalt mixtures and energy consumption could be reduced.
(2) In comparison to virgin asphalt, 40% aged asphalt containing maltene was more predisposed towards short-term ageing, as per the results of the RTFO test.
(3) Using maltene as a rejuvenator was shown to enhance the rheological properties of aged asphalt. These results were supported by the DSR and BBR measurements at high and low temperatures, respectively.
(4) The FTIR analysis confirmed that both maltene and asphalt did not chemically react during rejuvenation. The observed reduction of carbonyl and sulfoxide in rejuvenated asphalt was ascribed to the inclusion of maltene as a rejuvenator.
(5) The AFM images disclosed that the ageing process had changed the microstructure properties of asphalt. The addition of maltene had mitigated the aggregation of highly-oxidized components in asphalt and rejuvenated the aged asphalt to some degree.
(6) The rejuvenated asphalt revealed the higher temperature sensitiveness than the aged asphalt in addition to the resistance to thermal decomposition was very close to the virgin asphalt.
(7) The blend containing 40% of aged asphalt and 12% of maltene was demonstrated to be suitable for the successful recycling of the pavement.
(8) By carefully controlling the content of maltene in aged asphalt; the physical, rheological, and chemical characteristics can be customised to promote sustainable development within the civil construction sector.
(9) To better understanding the maltene effect as rejuvenator, it is essential to study the effects of ageing (both short – and long-term) after rejuvenation process. The mechanical performance

of rejuvenated asphalt mixtures should be further investigated to determine the rejuvenation potential.

Disclosure statement

Funding

ORCID

Ramadhansyah Putra Jaya http://orcid.org/0000-0002-5255-9856

References

AASHTO T240. (2013). *Standard method of test for effect of heat and air on a moving film of asphalt binder (Rolling Thin-Film Oven test)*. American Association of State Highway and Transportation Officials.

Aguiar-Moya, J. P., Salazar-Delgado, J., García, A., Baldi-Sevilla, A., Bonilla-Mora, V., & Loría-Salazar, L. G. (2017). Effect of ageing on micromechanical properties of bitumen by means of atomic force microscopy. *Road Materials and Pavement Design*, *18*(sup2), 203–215. https://doi.org/10.1080/14680629.2017.1304249

Al-Bayati, H. K. A., Tighe, S. L., & Achebe, J. (2018). Influence of recycled concrete aggregate on volumetric properties of hot mix asphalt. *Resources, Conservation and Recycling*, *130*, 200–214. https://doi.org/10.1016/j.resconrec.2017.11.027

Ali, A. W., Mehta, Y. A., Nolan, A., Purdy, C., & Bennert, T. (2016). Investigation of the impacts of aging and RAP percentages on effectiveness of asphalt binder rejuvenators. *Construction and Building Materials*, *110*, 211–217. https://doi.org/10.1016/j.conbuildmat.2016.02.013

Allen, R. G., Little, D. N., Bhasin, A., & Glover, C. J. (2014). The effects of chemical composition on asphalt microstructure and their association to pavement performance. *International Journal of Pavement Engineering*, *15*(1), 9–22. https://doi.org/10.1080/10298436.2013.836192

Al-Saffar, Z. H., Yaacob, H., Mohd Satar, M. K. I., Saleem, M. K., Putra Jaya, R., Lai, C. J., & Shaffie, E. (2020). Evaluating the chemical and rheological attributes of aged asphalt: Synergistic effects of maltene and waste engine oil rejuvenating agents. *Arabian Journal for Science and Engineering*, *45*(10), 8685–8697. https://doi.org/10.1007/s13369-020-04842-7 doi:10.1007/s13369-020-04842-7

Al-Saffar, Z. H., Yaacob, H., Satar, M. K. I. M., Saleem, M. K., Lai, J. C., & Putra Jaya, R. (2021). A review on rejuvenating materials used with reclaimed hot mix asphalt. *Canadian Journal of Civil Engineering*, *99*(999), 1–17. https://doi.org/10.1139/cjce-2019-0635

Alvarez, C. (1994). *Aging phenomenon in asphalt concrete pavements: A literature review*. University of Illinois, Department of Civil Engineering.

ASTM. (2016). *ASTM D6648-16, standard test method for determining the flexural creep stiffness of asphalt binder using the bending beam rheometer (BBR)*. ASTM International.

ASTM D113. (2017a). *Standard test method for ductility of asphalt materials. Annual book of ASTM standards*. ASTM International.

ASTM D2172 / D2172M. (2017b). *Standard test methods for quantitative extraction of asphalt binder from asphalt mixtures. Annual book of ASTM standards*. ASTM International.

ASTM D2872. (2012a). *Standard test method for effect of heat and air on a moving film of asphalt (Rolling Thin-Film Oven test): Annual book of ASTM standards*. ASTM International.

ASTM D36M. (2014). *Standard test method for softening point of bitumen (ring-and-ball apparatus): Annual book of ASTM standards*. ASTM International.

ASTM D4124. (2018). *Standard test method for separation of asphalt into four fractions. Annual book of ASTM standards*. ASTM International.

ASTM D4402/D4402M. (2015). *Standard test method for viscosity determination of asphalt at elevated temperatures using a rotational viscometer: Annual book of ASTM standards*. ASTM International.

ASTM D5404 / D5404M. (2012b). *Standard practice for recovery of asphalt from solution using the rotary evaporator: Annual book of ASTM standards*. ASTM International.

ASTM D5 / D5M. (2013). *Standard test method for penetration of bituminous materials. Annual book of ASTM standards*. ASTM International.

ASTM D7175-15. (2015b). *Standard test method for determining the rheological properties of asphalt binder using a dynamic shear rheometer: Annual book of ASTM standards*. ASTM International.

ASTM E1131. (2014). *Standard test method for compositional analysis by thermogravimetry. Annual book of ASTM standards*. ASTM International.

Aurangzeb, Q., Al-Qadi, I. L., Ozer, H., & Yang, R. (2014). Hybrid life cycle assessment for asphalt mixtures with high RAP content. *Resources, Conservation and Recycling*, *83*, 77–86. https://doi.org/10.1016/j.resconrec.2013.12.004

Bach, Q.-V., & Chen, W.-H. (2017). Pyrolysis characteristics and kinetics of microalgae via thermogravimetric analysis (TGA): A state-of-the-art review. *Bioresource Technology*, *246*, 88–100. https://doi.org/10.1016/j.biortech.2017.06.087

Backx, B. P., Simão, R. A., Dourado, E. R., & Leite, L. F. M. (2014). Solvent effect on the morphology of the bee: Structure observed by atomic force microscopy on bitumen sample. *Materials Research*, *17*(5), 1157–1161. https://doi.org/10.1590/1516-1439.236113 doi:10.1590/1516-1439.236113

Blanc, J., Hornych, P., Sotoodeh-Nia, Z., Williams, C., Porot, L., Pouget, S., Boysen, R., Planche, J.-P., Lo Presti, D., Jimenez, A., & Chailleux, E. (2019). Full-scale validation of bio-recycled asphalt mixtures for road pavements. *Journal of Cleaner Production*, *227*, 1068–1078. https://doi.org/10.1016/j.jclepro.2019.04.273

Borhan, M. N., Suja, E., Ismail, A., & Rahmat, R. A. O. (2007). Used cylinder oil modified cold—mix asphalt concrete. *Journal of Applied Sciences*, *7*(22), 3485–3491. https://doi.org/10.3923/jas.2007.3485.3491

Bylikin, S., Horner, G., Murphy, B., & Tarcy, D. (2014). *Chemistry: Course companion*. Oxford University Press.

Cao, X., Wang, H., Cao, X., Sun, W., Zhu, H., & Tang, B. (2018). Investigation of rheological and chemical properties asphalt binder rejuvenated with waste vegetable oil. *Construction and Building Materials*, *180*, 455–463. https://doi.org/10.1016/j.conbuildmat.2018.06.001

Cavalli, M. C., Zaumanis, M., Mazza, E., Partl, M. N., & Poulikakos, L. D. (2018). Effect of ageing on the mechanical and chemical properties of binder from RAP treated with bio-based rejuvenators. *Composites Part B: Engineering*, *141*, 174–181. https://doi.org/10.1016/j.compositesb.2017.12.060

Celauro, C., Bernardo, C., & Gabriele, B. (2010). Production of innovative, recycled and high-performance asphalt for road pavements. *Resources, Conservation and Recycling*, *54*(6), 337–347. https://doi.org/10.1016/j.resconrec.2009.08.009

Ciryle, S. S., Alexandre, P., & Emmanuel, C. (2016). Evaluation of the potential use of waste sunflower and rapeseed oils-modified natural bitumen as binders for asphalt pavement design. *International Journal of Pavement Research and Technology*, *9*(5), 368–375. https://doi.org/10.1016/j.ijprt.2016.09.001

Cuadri, A., García-Morales, M., Navarro, F., & Partal, P. (2014). Processing of bitumens modified by a bio-oil-derived polyurethane. *Fuel*, *118*, 83–90. https://doi.org/10.1016/j.fuel.2013.10.068

Elkashef, M., & Williams, R. C. (2017). Improving fatigue and low temperature performance of 100% RAP mixtures using a soybean-derived rejuvenator. *Construction and Building Materials*, *151*, 345–352. https://doi.org/10.1016/j.conbuildmat.2017.06.099

Elkashef, M., Williams, R. C., & Cochran, E. (2018). Thermal stability and evolved gas analysis of rejuvenated reclaimed asphalt pavement (RAP) bitumen using thermogravimetric analysis–Fourier transform infrared (TG–FTIR). *Journal of Thermal Analysis and Calorimetry*, *131*(2), 865–871. https://doi.org/10.1007/s10973-017-6674-9

Elseifi, M. A., Mohammad, L. N., & Cooper III, S. B. (2011). Laboratory evaluation of asphalt mixtures containing sustainable technologies. *Asphalt Paving Technology*, *80*, 227–244.

Feng, Z.-g., Bian, H.-j., Li, X.-j., & Yu, J.-y. (2016). FTIR analysis of UV aging on bitumen and its fractions. *Materials and Structures*, *49*(4), 1381–1389. https://doi.org/10.1617/s11527-015-0583-9

Firoozifar, S. H., Foroutan, S., & Foroutan, S. (2011). The effect of asphaltene on thermal properties of bitumen. *Chemical Engineering Research and Design*, *89*(10), 2044–2048. https://doi.org/10.1016/j.cherd.2011.01.025

Fursule, R. (2008). *Biochemistry basics And applied*. Pragati Books Pvt. Ltd.

Ghavibazoo, A., Abdelrahman, M., & Ragab, M. (2013). Mechanism of crumb rubber modifier dissolution into asphalt matrix and its effect on final physical properties of crumb rubber–modified binder. *Transportation Research Record: Journal of the Transportation Research Board*, *2370*(1), 92–101. https://doi.org/10.3141/2370-12

Gong, M., Yang, J., Zhang, J., Zhu, H., & Tong, T. (2016). Physical–chemical properties of aged asphalt rejuvenated by bio-oil derived from biodiesel residue. *Construction and Building Materials*, *105*, 35–45. https://doi.org/10.1016/j.conbuildmat.2015.12.025

Hofko, B., Alavi, M. Z., Grothe, H., Jones, D., & Harvey, J. (2017). Repeatability and sensitity of FTIR ATR spectral analysis methods for bituminous binders. *Materials and Structures*, *50*(3), 187. https://doi.org/10.1617/s11527-017-1059-x

Hofko, B., Eberhardsteiner, L., Füssl, J., Grothe, H., Handle, F., Hospodka, M., Grossegger, D., Nahar, S. N., Schmets, A. J. M., & Scarpas, A. (2016). Impact of maltene and asphaltene fraction on mechanical behavior and microstructure of bitumen. *Materials and Structures*, *49*(3), 829–841. https://doi.org/10.1617/s11527-015-0541-6

Hofko, B., Porot, L., Cannone, A. F., Poulikakos, L., Huber, L., Lu, X., Mollenhauer, K., & Grothe, H. (2018). FTIR spectral analysis of bituminous binders: Reproducibility and impact of ageing temperature. *Materials and Structures*, *51*(2), 45. https://doi.org/10.1617/s11527-018-1170-7

Hu, W., Shu, X., & Huang, B. (2019). Sustainability innovations in transportation infrastructure: An overview of the special volume on sustainable road paving. *Journal of Cleaner Production*, *235*, 369–377. https://doi.org/10.1016/j.jclepro.2019.06.258

Huang, S.-C., & Turner, T. F. (2013). Aging characteristics of RAP blend binders: Rheological properties. *Journal of Materials in Civil Engineering*, *26*(5), 966–973. https://doi.org/10.1061/(ASCE)MT.1943-5533.0000898

Hussein, Z., Yaacob, H., Idham, M., Abdulrahman, S., Choy, L., & Jaya, R. (2020a). Rejuvenation of hot mix asphalt incorporating high RAP content: Issues to consider. *IOP Conference Series: Earth and Environmental Science*, *498*(1). https://doi.org/10.1088/1755-1315/498/1/012009

Hussein, Z., Yaacob, H., Idham, M., Hassan, N., Choy, L., & Jaya, R. (2020b). Restoration of aged bitumen properties using maltenes. *IOP Conference Series: Materials Science and Engineering*, *713*, 012014. https://doi.org/10.1088/1757-899X/713/1/012014

Ingrassia, L. P., Lu, X., Ferrotti, G., & Canestrari, F. (2019). Renewable materials in bituminous binders and mixtures: Speculative pretext or reliable opportunity? *Resources, Conservation and Recycling*, *144*, 209–222. https://doi.org/10.1016/j.resconrec.2019.01.034

Ji, J., Yao, H., Suo, Z., You, Z., Li, H., Xu, S., & Sun, L. (2017). Effectiveness of vegetable oils as rejuvenators for aged asphalt binders. *Journal of Materials in Civil Engineering*, *29*(3), D4016003. https://doi.org/10.1061/(ASCE)MT.1943-5533.0001769

Jia, X., Huang, B., Moore, J. A., & Zhao, S. (2015). Influence of waste engine oil on asphalt mixtures containing reclaimed asphalt pavement. *Journal of Materials in Civil Engineering*, *27*(12), 04015042. https://doi.org/10.1061/(ASCE)MT.1943-5533.0001292

Jiménez-Mateos, J. M., Quintero, L. C., & Rial, C. (1996). Characterization of petroleum bitumens and their fractions by thermogravimetric analysis and differential scanning calorimetry. *Fuel*, *75*(15), 1691–1700. https://doi.org/10.1016/S0016-2361(96)00169-X

Kaseer, F., Martin, A. E., & Arámbula-Mercado, E. (2019). Use of recycling agents in asphalt mixtures with high recycled materials contents in the United States: A literature review. *Construction and Building Materials*, *211*, 974–987. https://doi.org/10.1016/j.conbuildmat.2019.03.286

Lamontagne, J., Dumas, P., Mouillet, V., & Kister, J. (2001). Comparison by Fourier transform infrared (FTIR) spectroscopy of different ageing techniques: Application to road bitumens. *Fuel*, *80*(4), 483–488. https://doi.org/10.1016/S0016-2361(00)00121-6

Lillian Gungat, M. O. H., Hasan, M. R. M., & Valentin, J. (2018). Warm mix and reclaimed asphalt pavement: A greener road approach. *International Scholarly and Scientific Research & Innovation*, *12*(11), 1107–1112. DOI: doi.org/10.5281/zenodo.2021873

Ma, T., Wang, H., Huang, X., Wang, Z., & Xiao, F. (2015). Laboratory performance characteristics of high modulus asphalt mixture with high-content RAP. *Construction and Building Materials*, *101*, 975–982. https://doi.org/10.1016/j.conbuildmat.2015.10.160

Magonov, S., Alexander, J., Surtchev, M., Hung, A. M., & Fini, E. H. (2017). Compositional mapping of bitumen using local electrostatic force interactions in atomic force microscopy. *Journal of Microscopy*, *265*(2), 196–206. https://doi.org/10.1111/jmi.12475

Mansourkhaki, A., Ameri, M., & Daryaee, D. (2019). Application of different modifiers for improvement of chemical characterization and physical-rheological parameters of reclaimed asphalt binder. *Construction and Building Materials*, *203*, 83–94. https://doi.org/10.1016/j.conbuildmat.2019.01.086

Mirwald, J., Werkovits, S., Camargo, I., Maschauer, D., Hofko, B., & Grothe, H. (2020a). Investigating bitumen long-term-ageing in the laboratory by spectroscopic analysis of the SARA fractions. *Construction and Building Materials*, *258*. https://doi.org/10.1016/j.conbuildmat.2020.119577

Mirwald, J., Werkovits, S., Camargo, I., Maschauer, D., Hofko, B., & Grothe, H. (2020b). Understanding bitumen ageing by investigation of its polarity fractions. *Construction and Building Materials*, *250*. https://doi.org/10.1016/j.conbuildmat.2020.118809

Moghaddam, T. B., & Baaj, H. (2016). The use of rejuvenating agents in production of recycled hot mix asphalt: A systematic review. *Construction and Building Materials*, *114*, 805–816. https://doi.org/10.1016/j.conbuildmat.2016.04.015

Mouazen, M., Poulesquen, A., & Vergnes, B. (2011). Influence of thermomechanical history on chemical and rheological behavior of bitumen. *Energy & Fuels*, *25*(10), 4614–4621. https://doi.org/10.1021/ef201000j doi:10.1021/ef201000j

Mouillet, V., Lamontagne, J., Durrieu, F., Planche, J.-P., & Lapalu, L. (2008). Infrared microscopy investigation of oxidation and phase evolution in bitumen modified with polymers. *Fuel*, *87*(7), 1270–1280. https://doi.org/10.1016/j.fuel.2007.06.029

Mousavi, M., Pahlavan, F., Oldham, D., Hosseinnezhad, S., & Fini, E. H. (2016). Multiscale investigation of oxidative aging in biomodified asphalt binder. *The Journal of Physical Chemistry C*, *120*(31), 17224–17233. https://doi.org/10.1021/acs.jpcc.6b05004

Noferini, L., Simone, A., Sangiorgi, C., & Mazzotta, F. (2017). Investigation on performances of asphalt mixtures made with reclaimed asphalt pavement: Effects of interaction between virgin and RAP bitumen. *International Journal of Pavement Research and Technology*, *10*(4), 322–332. https://doi.org/10.1016/j.ijprt.2017.03.011

Pauli, A., Grimes, R., Beemer, A., Turner, T., & Branthaver, J. (2011). Morphology of asphalts, asphalt fractions and model wax-doped asphalts studied by atomic force microscopy. *International Journal of Pavement Engineering*, *12*(4), 291–309. https://doi.org/10.1080/10298436.2011.575942

Pellinen, T. K., Witczak, M. W., & Bonaquist, R. F. (2004). Asphalt mix master curve construction using sigmoidal fitting function with non-linear least squares optimization. *Recent advances in materials characterization and modeling of pavement systems* (pp. 83–101). https://doi.org/10.1061/40709(257)6

Pizzorno, B., Dourado, E., Moraes, M. d., Simão, R., & Leite, L. (2014). Segregation and crystallization of waxes on the surface of asphalt binders as observed by atomic force microscopy. *Petroleum Science and Technology*, *32*(22), 2738–2745. https://doi.org/10.1080/10916466.2014.887099

Poulikakos, L., Papadaskalopoulou, C., Hofko, B., Gschösser, F., Falchetto, A. C., Bueno, M., Arraigada, M., Sousa, J., Ruiz, R., Petit, C., Loizidou, M., & Partl, M. N. (2017). Harvesting the unexplored potential of European waste materials for road construction. *Resources, Conservation and Recycling*, 116, 32–44. https://doi.org/10.1016/j.resconrec.2016.09.008

Roberts, F. L., Kandhal, P. S., Brown, E. R., Lee, D.-Y., & Kennedy, T. W. (1991). *Hot mix asphalt materials, mixture design and construction*. Lanham, MD: NAPA Research and Education Foundation.

Rodríguez-Fernández, I., Lastra-González, P., Indacoechea-Vega, I., & Castro-Fresno, D. (2019). Recyclability potential of asphalt mixes containing reclaimed asphalt pavement and industrial by-products. *Construction and Building Materials*, 195, 148–155. https://doi.org/10.1016/j.conbuildmat.2018.11.069

Salomon, D., & Zhai, H. (2002). Ranking asphalt binders by activation energy for flow. *Journal of Applied Asphalt Binder Technology*, 2(2), 52–60.

Southern, M. (2015). A perspective of bituminous binder specifications. In Editors: Shin-Che Huang Hervé Di Benedetto (Ed.), *Advances in asphalt materials* (pp. 1–27). Elsevier.

Su, K., Hachiya, Y., & Maekawa, R. (2009). Study on recycled asphalt concrete for use in surface course in airport pavement. *Resources, Conservation and Recycling*, 54(1), 37–44. https://doi.org/10.1016/j.resconrec.2009.06.003

Tahmoorian, F., Samali, B., & Yeaman, J. (2018). Evaluation of structural and thermal properties of rubber and HDPE for utilization as binder modifier. *Modified Asphalt*, 109, 109–127. https://doi.org/10.5772/intechopen.75535

Tan, Y., & Guo, M. (2013). Study on the phase behavior of asphalt mastic. *Construction and Building Materials*, 47, 311–317. https://doi.org/10.1016/j.conbuildmat.2013.05.064

Wang, F., Fang, Y., Chen, Z., & Wei, H. (2018). Effect of waste engine oil on asphalt reclaimed properties. In *AIP conference proceedings* (Vol. 1973, p. 020012): AIP Publishing. https://doi.org/10.1063/1.5041396

Wang, M., & Liu, L. (2017). Investigation of microscale aging behavior of asphalt binders using atomic force microscopy. *Construction and Building Materials*, 135, 411–419. https://doi.org/10.1016/j.conbuildmat.2016.12.180

Wang, W., Chen, J., Sun, Y., Xu, B., Li, J., & Liu, J. (2017). Laboratory performance analysis of high percentage artificial RAP binder with WMA additives. *Construction and Building Materials*, 147, 58–65. https://doi.org/10.1016/j.conbuildmat.2017.04.142

Wang, Z., & Ye, F. (2020). Experimental investigation on aging characteristics of asphalt based on rheological properties. *Construction and Building Materials*, 231, 117158. https://doi.org/10.1016/j.conbuildmat.2019.117158

Xiaohu, L., & Isacsson, U. (2002). Effect of ageing on bitumen chemistry and rheology. *Construction and Building Materials*, 16(1), 15–22. https://doi.org/10.1016/S0950-0618(01)00033-2

Yan, C., Huang, W., & Lv, Q. (2016). Study on bond properties between RAP aggregates and virgin asphalt using binder bond strength test and Fourier transform infrared spectroscopy. *Construction and Building Materials*, 124, 1–10. https://doi.org/10.1016/j.conbuildmat.2016.07.024

Yang, R., Kang, S., Ozer, H., & Al-Qadi, I. L. (2015). Environmental and economic analyses of recycled asphalt concrete mixtures based on material production and potential performance. *Resources, Conservation and Recycling*, 104, 141–151. https://doi.org/10.1016/j.resconrec.2015.08.014

Yu, X., Zaumanis, M., Dos Santos, S., & Poulikakos, L. D. (2014). Rheological, microscopic, and chemical characterization of the rejuvenating effect on asphalt binders. *Fuel*, 135(1), 162–171. https://doi.org/10.1016/j.fuel.2014.06.038

Zargar, M., Ahmadinia, E., Asli, H., & Karim, M. R. (2012). Investigation of the possibility of using waste cooking oil as a rejuvenating agent for aged bitumen. *Journal of Hazardous Materials*, 233-234, 254–258. https://doi.org/10.1016/j.jhazmat.2012.06.021

Zaumanis, M., & Mallick, R. B. (2015). Review of very high-content reclaimed asphalt use in plant-produced pavements: State of the art. *International Journal of Pavement Engineering*, 16(1), 39–55. https://doi.org/10.1080/10298436.2014.893331

Zaumanis, M., Mallick, R. B., & Frank, R. (2013). Evaluation of rejuvenator's effectiveness with conventional mix testing for 100% reclaimed asphalt pavement mixtures. *Transportation Research Record: Journal of the Transportation Research Board*, 2370(1), 17–25. https://doi.org/10.3141/2370-03

Zaumanis, M., Mallick, R. B., & Frank, R. (2014a). 100% recycled hot mix asphalt: A review and analysis. *Resources, Conservation and Recycling*, 92, 230–245. https://doi.org/10.1016/j.resconrec.2014.07.007

Zaumanis, M., Mallick, R. B., Poulikakos, L., & Frank, R. (2014b). Influence of six rejuvenators on the performance properties of reclaimed asphalt pavement (RAP) binder and 100% recycled asphalt mixtures. *Construction and Building Materials*, 71, 538–550. https://doi.org/10.1016/j.conbuildmat.2014.08.073

Zhang, R., You, Z., Wang, H., Chen, X., Si, C., & Peng, C. (2018a). Using bio-based rejuvenator derived from waste wood to recycle old asphalt. *Construction and Building Materials*, 189, 568–575. https://doi.org/10.1016/j.conbuildmat.2018.08.201

Zhang, R., You, Z., Wang, H., Ye, M., Yap, Y. K., & Si, C. (2019). The impact of bio-oil as rejuvenator for aged asphalt binder. *Construction and Building Materials*, 196, 134–143. https://doi.org/10.1016/j.conbuildmat.2018.10.168

Zhang, Z., Jia, M., Jiao, W., Qi, B., & Liu, H. (2018b). Physical properties and microstructures of organic rectorites and their modified asphalts. *Construction and Building Materials*, 171, 33–43. https://doi.org/10.1016/j.conbuildmat.2018.01.163

Zhu, H., Xu, G., Gong, M., & Yang, J. (2017). Recycling long-term-aged asphalts using bio-binder/plasticizer-based rejuvenator. *Construction and Building Materials*, 147, 117–129. https://doi.org/10.1016/j.conbuildmat.2017.04.066